Article

Cell Stem Cell

Bmi1 Is a Key Epigenetic Barrier to Direct Cardiac Reprogramming

Graphical Abstract

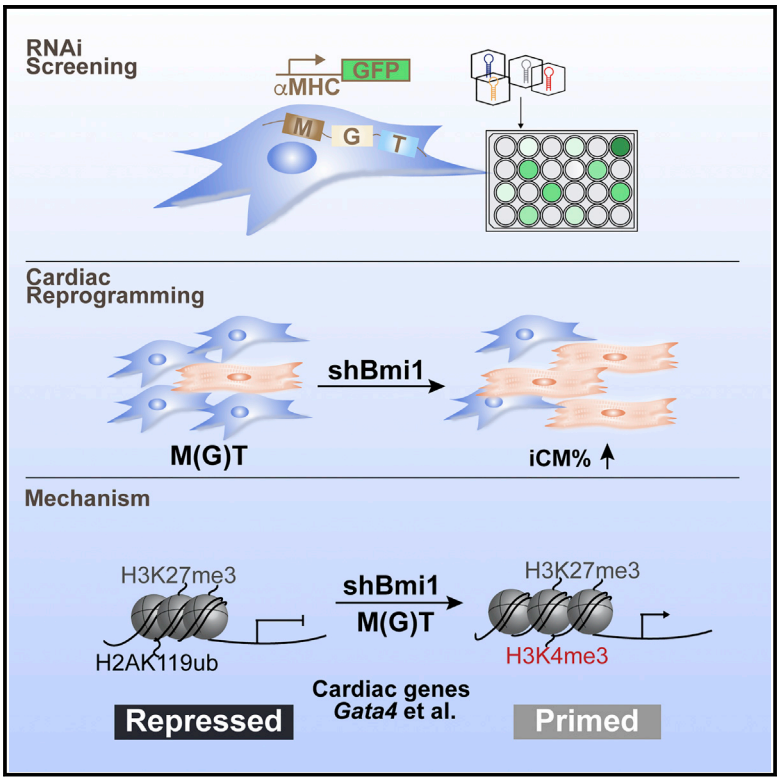

Authors

Yang Zhou, Li Wang, Haley Ruth Vaseghi, ..., Greg G. Wang, Jiandong Liu, Li Qian

Correspondence

li_qian@med.unc.edu

In Brief

Qian and colleagues carried out a loss-of-function screen to identify epigenetic factors that modulate reprogramming of fibroblasts into beating cardiomyocytes. They found that repression of Bmi1 enhances reprogramming efficiency and correlates with altered epigenetic status at key cardiogenic loci, resulting in their de-repression.

Highlights

- shRNA screen identified Bmi1 as a major epigenetic barrier to cardiac reprogramming
- Bmi1 downregulation significantly enhanced iCM generation from mouse fibroblasts
- Bmi1 directly binds to and suppresses cardiogenic loci
- Bmi1 depletion can functionally substitute for Gata4 during iCM conversion

Zhou et al., 2016, Cell Stem Cell *18*, 382–395
March 3, 2016 ©2016 Elsevier Inc.
http://dx.doi.org/10.1016/j.stem.2016.02.003

CellPress

Cell Stem Cell
Article

Bmi1 Is a Key Epigenetic Barrier to Direct Cardiac Reprogramming

Yang Zhou,[1,2] Li Wang,[1,2] Haley Ruth Vaseghi,[1,2] Ziqing Liu,[1,2] Rui Lu,[3] Sahar Alimohamadi,[1,2] Chaoying Yin,[1,2] Ji-Dong Fu,[4] Greg G. Wang,[3,5] Jiandong Liu,[1,2] and Li Qian[1,2,*]

[1]Department of Pathology and Laboratory Medicine, University of North Carolina, Chapel Hill, NC 27599, USA
[2]McAllister Heart Institute, University of North Carolina, Chapel Hill, NC 27599, USA
[3]Lineberger Comprehensive Cancer Center, University of North Carolina, Chapel Hill, NC 27599, USA
[4]Department of Medicine, Heart and Vascular Research Center, MetroHealth Campus, Case Western Reserve University, Cleveland, OH 44109, USA
[5]Department of Biochemistry and Biophysics, University of North Carolina, Chapel Hill, NC 27599, USA
*Correspondence: li_qian@med.unc.edu
http://dx.doi.org/10.1016/j.stem.2016.02.003

SUMMARY

Direct reprogramming of induced cardiomyocytes (iCMs) suffers from low efficiency and requires extensive epigenetic repatterning, although the underlying mechanisms are largely unknown. To address these issues, we screened for epigenetic regulators of iCM reprogramming and found that reducing levels of the polycomb complex gene *Bmi1* significantly enhanced induction of beating iCMs from neonatal and adult mouse fibroblasts. The inhibitory role of Bmi1 in iCM reprogramming is mediated through direct interactions with regulatory regions of cardiogenic genes, rather than regulation of cell proliferation. Reduced *Bmi1* expression corresponded with increased levels of the active histone mark H3K4me3 and reduced levels of repressive H2AK119ub at cardiogenic loci, and de-repression of cardiogenic gene expression during iCM conversion. Furthermore, *Bmi1* deletion could substitute for Gata4 during iCM reprogramming. Thus, Bmi1 acts as a critical epigenetic barrier to iCM production. Bypassing this barrier simplifies iCM generation and increases yield, potentially streamlining iCM production for therapeutic purposes.

INTRODUCTION

The adult mammalian heart has limited regenerative capacity and is thus an important target for novel regenerative approaches to replenish lost cardiomyocytes (CMs) after cardiac injury (Laflamme and Murry, 2011; Porrello et al., 2011; Ubil et al., 2014; Xin et al., 2013). Cardiac reprogramming that converts fibroblasts to contractile induced cardiomyocytes (iCMs) by overexpression of cardiac-lineage-specific transcription factors holds great promise as an alternative approach for cardiac regeneration and disease modeling (Addis and Epstein, 2013; Addis et al., 2013; Chen et al., 2012; Fu et al., 2013; Hirai et al., 2013; Ieda et al., 2010; Ifkovits et al., 2014; Jayawardena et al., 2012; Muraoka et al., 2014; Nam et al., 2013; Protze et al., 2012; Qian and Srivastava, 2013; Song et al., 2012; Wada et al., 2013; Wang et al., 2015a; Zhao et al., 2015; Zhou et al., 2015). However, our limited understanding of the molecular mechanism underlying cardiac reprogramming has significantly hindered its potential translational applications.

Epigenetic regulation plays a critical role in shaping and maintaining cellular identities during developmental programming and cellular reprogramming. Recent studies on in vitro cardiac differentiation of embryonic stem cells demonstrated that temporal activation of functionally important cardiac genes requires coordinated programmed control of chromatin structure (Paige et al., 2012; Wamstad et al., 2012). Likewise, cellular reprogramming is accompanied by profound changes in the epigenetic landscape (Dhawan et al., 2011; Liang and Zhang, 2013; Luna-Zurita and Bruneau, 2013; Onder et al., 2012; Tursun et al., 2011). This transition in epigenetic status is likely to be involved in suppressing the original cell-type-specific signature and establishing and stabilizing a target cell-type-specific program (Apostolou and Hochedlinger, 2013; Buganim et al., 2013; Papp and Plath, 2013). Epigenetic alterations were also observed at both fibroblast- and CM-specific marker genes during iCM reprogramming (Fu et al., 2013; Ieda et al., 2010). However, how these epigenetic transitions are regulated remains elusive. iCM reprogramming, like other types of cellular reprogramming, is an inefficient and slow process, which is at least in part due to multiple epigenetic barriers that have not been identified. It also remains unclear whether iCM reprogramming shares similar epigenetic mechanisms with induced pluripotent stem cell (iPSC) reprogramming or has its own specific barriers.

Here we report the first shRNA-based loss-of-function screen to explore the role of epigenetic factors in iCM reprogramming. Among the identified epigenetic regulators of iCM reprogramming, the polycomb ring finger oncogene *Bmi1* acted as a major epigenetic barrier during the early phase of iCM reprogramming. Genetic and epistasis analyses suggested that the inhibitory effect of Bmi1 on iCM reprogramming was not completely mediated by its downstream effectors involved in cell proliferation such as $p16^{Ink4a}$, $p19^{Arf}$, and *p53*. Instead, we discovered an uncharacterized role of Bmi1 in directly binding the regulatory regions of several cardiogenic genes including *Gata4*. Knockdown of *Bmi1* caused de-repression of endogenous *Gata4* and could

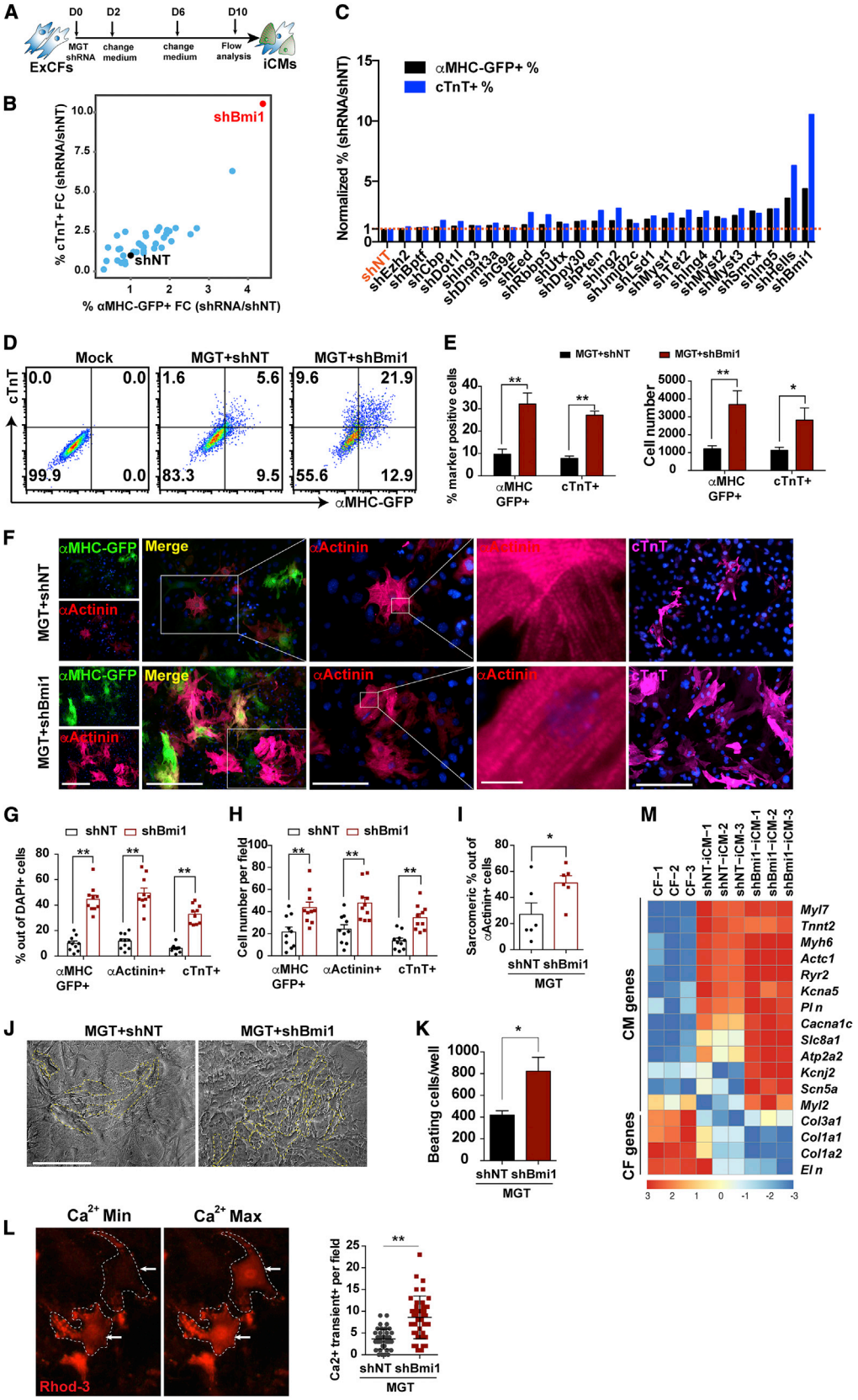

(legend on next page)

functionally replace Gata4 to induce beating iCMs. Thus, our work identifies Bmi1 as a critical epigenetic barrier at the early stage of iCM reprogramming and demonstrates that removing this early epigenetic barrier is sufficient to generate functional iCMs with fewer transcription factors.

RESULTS

Loss-of-Function Screen Identified Epigenetic Barriers to, and Facilitators of, iCM Reprogramming

To identify potential epigenetic regulators of iCM reprogramming, we employed a loss-of-function approach to explore the function of 35 selected components of chromatin modifying or remodeling complexes (Table S1). For each candidate, a pool of shRNAs (four to six independent shRNA constructs) targeting different regions within the gene was used and knockdown efficiency was validated (Table S1 and Figure S1A). The individual shRNA pools were then transduced into neonatal cardiac fibroblasts (CFs) isolated by using explant culture method (ExCFs) from a transgenic α-muscle heavy chain (αMHC)-GFP reporter mouse (Ieda et al., 2010; Qian et al., 2013) together with retroviruses expressing polycistronic Mef2c/Gata4/Tbx5 (MGT) (Wang et al., 2015a). Upon transduction of MGT, activation of GFP allowed us to follow the emergence of newly induced iCMs. Furthermore, we used cardiac Troponin T (cTnT) as an additional differentiated CM marker to monitor CF to CM fate conversion (Figure 1A). iCM reprogramming efficiency was determined by flow cytometry analysis to quantify the percentage of αMHC-GFP+ and cTnT+ cells (Figure 1A). Although to various degrees, knocking down 11 of the 35 epigenetic regulators reduced reprogramming efficiency (Figure 1B and Table S1). Silencing inhibitor of growth family member 1 (*Ing1*) or lysine (K)-specific demethylase 5B (*Kdm5b/Plu1*) resulted in at least 2-fold reduction in the percentages of αMHC-GFP+ or cTnT+ cells (Figure 1B and Table S1). Ing1 functions as a reader protein of H3K4me3/2, while Plu1 acts as an H3K4me3/2 demethylase (Table S1). These observations highlight the importance of histone methylation during iCM reprogramming. On the contrary, loss of Plu1 function has been found to enhance iPSC reprogramming (Kidder et al., 2013), suggesting that this histone modifier might be required for iCM reprogramming while impeding reprogramming to pluripotency.

In addition to the factors that were required for iCM reprogramming, we also identified epigenetic regulators that likely acted as barriers to iCM reprogramming (Figures 1B and 1C). shRNA pools against K(lysine) acetyltransferase 7 (*Kat7/Myst2*), K(lysine) acetyltransferase 6A (*Kat6a/Myst3*), lysine (K)-specific demethylase 5C (*Kdm5c/Smcx*) or inhibitor of growth family member 5 (*Ing5*) resulted in a roughly 2-fold increase in iCM reprogramming efficiency (Figure 1C and Table S1). Myst2 and Myst3 belong to the MYST family of histone acetyltransferases, whereas Smcx functions as an H3K4 demethylase (Table S1). Knockdown of helicase lymphoid specific (*Hells/Lsh/Smarca6*) resulted in a 6-fold increase in the percentage of cTnT+ cells (Figures 1B and 1C, Table S1). *Hells* encodes a component of the SWI/SNF complex, and targeted deletion of *Hells* leads to a genome-wide loss of DNA methylation and perinatal lethality (Geiman et al., 2001). In conclusion, chromatin regulatory factors involved in various aspects of epigenetic regulation function either as facilitators of or barriers to iCM reprogramming.

Bmi1 Acts as a Critical Epigenetic Barrier to iCM Reprogramming

Among the 35 candidate epigenetic regulators, ablation of *Bmi1*, which encodes a polycomb group protein homologous to *Drosophila* protein Posterior Sex Combs (Psc) (van Lohuizen et al., 1991; van der Lugt et al., 1994), resulted in the most significant increase in iCM reprogramming efficiency (Figures 1B and 1C, Table S1). Flow analysis and quantification showed that knocking down *Bmi1* led to a 10-fold increase in the percentage of cTnT+ cells (Figures 1B and 1C, Table S1). This significant enhancement of iCM reprogramming efficiency caused by loss of Bmi1 function is in sharp contrast to its positive role in iPSC reprogramming (Moon et al., 2011; Onder et al., 2012). Thus, we decided to focus on exploring the role of Bmi1 during fibroblast conversion into iCM. To further determine the effect of *Bmi1* knockdown on iCM reprogramming, we used two individual *Bmi1* shRNAs, along with MGT to convert neonatal ExCFs into iCMs. Consistently, silencing *Bmi1* with these two shRNAs individually resulted in a significant increase in the percentage of αMHC-GFP+ and cTnT+ cells compared to shNT controls (Figures S1B and S1C). Pooled shBmi1 oligos had a knockdown efficiency of >90% and increased iCM reprogramming efficiency to an even greater degree than individual shBmi1 oligos (Figures S1C and S1D). For the rest of the study, we used shBmi1-pool (referred to as shBmi1) unless otherwise indicated. shBmi1 treatment not only increased the percentage of iCMs but also

Figure 1. shRNA Screen Identified Bmi1 as a Critical Epigenetic Modulator of iCM Reprogramming

(A–C) shRNA screen for identifying epigenetic regulators of iCM reprogramming. (A) Schematic of the shRNA screen. (B) 2D scatter plot showing fold change (FC) in the percentage of αMHC-GFP+ and cTnT+ cells. (C) Histogram of normalized percentages of αMHC-GFP+ and cTnT+ cells from positive hits. ExCFs, explant cardiac fibroblasts; iCMs, induced cardiomyocytes; shNT, non-targeting shRNA control.

(D and E) Representative flow plots (D) and quantification (E) for αMHC-GFP+ and cTnT+ cells 10 days after MGT and shBmi1 or shNT transduction on freshly isolated CFs.

(F–I) Representative immunocytochemistry (ICC) images (F) for αMHC-GFP (green), αActinin (red), and cTnT (magenta) on MGT-transduced freshly isolated CFs infected with shNT or shBmi1, with quantification of the percentage in (G) and the absolute number in (H). High-magnification views of αActinin staining show sarcomere structures with quantification in (I). DAPI (blue) was used to stain nuclei. Scale bars, from left to right: 200 μm, 200 μm, 100 μm, 10 μm, and 200 μm.

(J and K) Representative images of spontaneously contracting iCMs (dotted lines) with indicated viral infection 4 weeks after being reprogrammed from freshly isolated CFs, corresponding to Movie S1 and Movie S2. Quantification of beating cells in one well of a 24-well plate is in (K).

(L) Representative images of iCMs exhibiting calcium transient (left panel) with quantification (right panel). iCMs were labeled with Rhod-3 4 weeks after MGT and shBmi1 transduction, corresponding to Movie S3.

(M) Heatmap of the relative expression of a set of CM and CF marker genes in control CFs and shNT- or shBmi1-infected ExCFs 2 weeks after MGT transduction.

For each experiment, n = ~3–6 (except n = 10 for G and H; n = 40 for L), and averaged numbers from technical duplicates or triplicates were used for statistics. Error bars indicate mean ± SEM; *p < 0.05, **p < 0.01. See also Figure S1.

resulted in an increased number of iCMs compared to shNT control treatment. We quantified the absolute numbers of αMHC-GFP+ or cTnT+ iCMs using flow cytometry and observed a significant increase in the numbers of both αMHC-GFP+ and cTnT+ cells (Figure S1E). Additionally, shBmi1-treated, freshly isolated neonatal CFs exhibited a similar increase in reprogramming efficiency and the numbers of αMHC-GFP+ or cTnT+ cells (Figures 1D and 1E).

We next determined if this increased CF to iCM conversion rate could translate into enhanced structural and functional maturation. We performed immunocytochemistry (ICC) on shBmi1- and shNT-treated cultures 2 weeks after infection and found that *Bmi1* knockdown resulted in a significantly increased number of cells expressing sarcomeric αActinin and cTnT (Figures 1F–1H). In addition, *Bmi1* knockdown gave rise to an 88.7% increase in the number of αActinin+ iCMs that assembled sarcomeres (Figure 1I). More strikingly, we observed twice as many beating iCMs that exhibited periodic calcium oscillation in shBmi1 cultures as we did in control cultures (Figures 1J–1L, Movie S1, Movie S2, and Movie S3). Furthermore, molecular characterization of the *Bmi1*-depleted and control cells by examination of the expression of a panel of sarcomere, contractility, and ion channel genes revealed higher expression of these functionally important cardiac genes in the *Bmi1*-depleted cultures (Figure 1M). Taken together, our data demonstrate that knockdown of *Bmi1* remarkably enhances MGT-mediated iCM reprogramming.

To further assess the repressive function of Bmi1 on cardiac reprogramming, we used the following three commonly used reprogramming methods in conjunction with shBmi1 or shNT to generate iCMs from freshly isolated neonatal CFs: (1) the MGT polycistronic construct (Wang et al., 2015a), (2) separate M+G+T (Ieda et al., 2010), or (3) M+G+T plus Hand2 (M+G+T+H) (Song et al., 2012). Interestingly, we observed the highest percentage of αMHC-GFP+ or cTnT+ cells by MGT, but the highest absolute number of cTnT+ cells by M+G+T+H regardless of *Bmi1* knockdown (Figures 2A–2F), reflecting varied reprogramming outcomes depending on which marker was used as the readout. Nevertheless, *Bmi1* knockdown uniformly increased iCM percentage across all reprogramming conditions (Figures 2A–2F) and exerted the most influence over the MGT transduced cultures (Figures 2A–2F). The significant increase in reprogramming efficiency observed with *Bmi1* knockdown under all conditions indicates that depletion of *Bmi1* influences cardiac reprogramming mediated by different cocktails and leads to higher reprogramming efficiency (reached to 50% of marker+ iCMs under MGT induction) compared to the corresponding controls.

Furthermore, we validated our findings in multiple cell types of diverse origin, including mouse embryonic fibroblasts (MEFs), neonatal tail tip fibroblasts (TTFs), adult CFs, adult TTFs, and CD31+ endothelial cells. Upon *Bmi1* knockdown, all cell types exhibited a significant increase in the percentage and absolute number of cardiac-marker-positive iCMs 10 days after MGT transduction (Figures 2G–2P). Quantification of flow and ICC analyses also revealed that enhancement of iCM induction varied depending on the cell types assayed (Figures 2G–2P), suggesting potential intrinsic variability of genetic and epigenetic features and cell plasticity among different cell types. To further validate the enhancement of cardiac reprogramming in non-fibroblast CD31+ endothelial cells, we assessed the expression of several sarcomere and ion channel markers, including *Myh6*, *Myl7*, *Actc1*, *Pln*, *Slc8a1*, *Scn5a*, *Cacna1c*, *Ryr2*, and *Myl2*, and we found that these markers were more highly expressed in shBmi1-treated cells, especially the ion channel marker genes (Figure S2A). Thus, *Bmi1* knockdown enhances iCM reprogramming under a variety of conditions and across diverse cell types.

Given the opposing effects of Bmi1 depletion on iCM reprogramming and iPSC reprogramming, we next asked if Bmi1 acted as a general repressor of somatic reprogramming/transdifferentiation or functioned specifically as a repressor of iCM reprogramming. To this end, we generated induced neurons (iNs) from MEFs by following a recently reported protocol (Xue et al., 2013) with shBmi1 or shNT. The efficiency of iN reprogramming was assessed using ICC of neuron marker microtubule associated protein 2 (MAP2) (Figure S2B). Although *Bmi1* knockdown appeared to alter the morphology of the MAP2+ iNs (Figure S2B), it did not have any effect on the number of MAP2+ cells (Figure S2C). Further analysis revealed that there was no significant change in the expression levels of additional neuronal markers such as class III β-tubulin (*Tubb3*) and Nestin (*Nes*) with shBmi1 compared to the control (Figure S2D). These results indicate that Bmi1 does not regulate direct neuron reprogramming but rather acts as a specific repressor of the iCM reprogramming.

Bmi1 Functions at the Early Stage of iCM Reprogramming

Next, we sought to determine the temporal window for silencing *Bmi1* to achieve an enhancement in iCM induction. We performed flow analysis and quantified the percentage of αMHC-GFP+ and cTnT+ cells generated from shBmi1- and shNT-treated reprogramming ExCFs at a series of time points. Enhancement in iCM reprogramming efficiency by shBmi1 occurred as early as day 3 (Figures 3A and 3B). Likewise, western blot analysis indicated that *Bmi1* depletion resulted in a significant upregulation of cardiac marker αMHC-GFP protein expression as early as day 3 (Figure 3C). These observations were further confirmed by the higher expression of a panel of CM marker genes in shBmi1-treated reprogramming fibroblasts at day 3, suggesting an effect of *Bmi1* knockdown on cardiac fate acquisition at the early stage of reprogramming (Figure 3D). To further define the critical time window for *Bmi1* knockdown, we introduced *Bmi1* shRNAs into neonatal ExCFs at 0, 1, 2, 3, or 5 days after MGT transduction (Figure 3E). Interestingly, we found that iCM reprogramming efficiency as indicated by the percentages of αMHC-GFP+ or cTnT+ cells was reliably increased only if shBmi1 was introduced within 3 days of MGT infection (Figures 3F and 3G). Depletion of *Bmi1* at 5 days after MGT transduction did not noticeably affect iCM generation (Figures 3F and 3G). Moreover, reasoning that chromatin remodeling is a prerequisite step to cell fate conversion, we asked if removing the epigenetic barrier by knocking down *Bmi1* prior to the introduction of MGT could lead to a similar enhancement. Fibroblasts were infected with shBmi1-puro lentiviruses and cultured under puromycin selection for 3 days before MGT transduction (Figure 3H). Flow cytometry analysis showed that shBmi1-treated neonatal ExCFs also had significantly higher

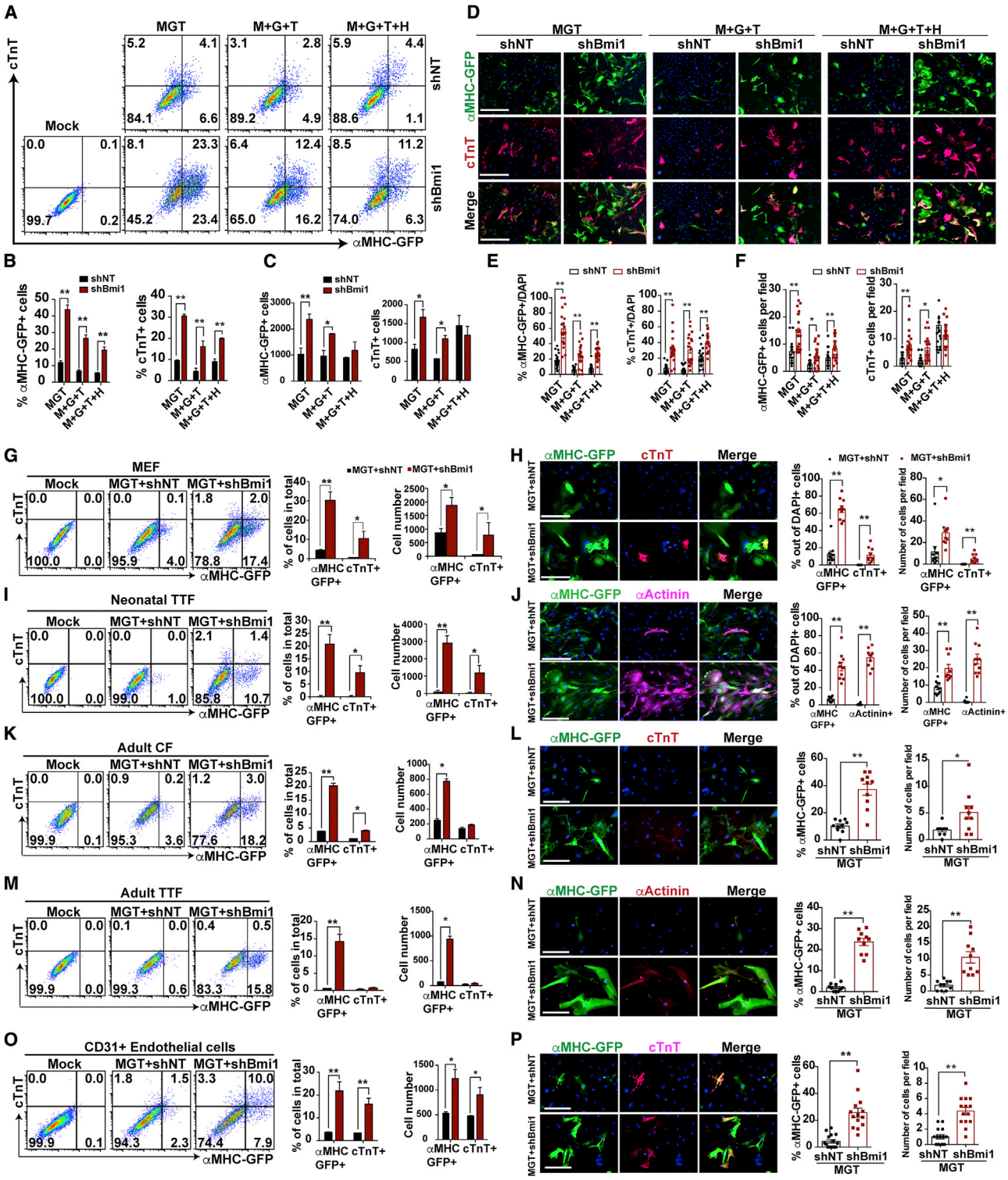

Figure 2. Knockdown of Bmi1 Enhanced the Conversion of Diverse Cell Types into iCM When Different Cocktails Were Used

(A–F) Representative flow plots with quantification (A–C) and ICC images with quantification (D–F) for αMHC-GFP+ and cTnT+ cells reprogrammed from fresh CFs 10 days after viral infection. DAPI (blue) was used to stain nuclei. Scale bars, 400 μm.

(G–P) Representative flow plots with quantification and ICC images with quantification for cardiac-marker-gene-positive cells (as indicated) reprogrammed from MEFs (G and H), neonatal TTFs (I and J), adult CFs (K and L), adult TTFs (M and N), and CD31+ endothelial cells (O and P) 10 days after viral infection. Scale bars, 200 μm. For each experiment, n = ~3–6 (except n = 20 for E and F; n = 10 for H, J, L, N, and P); averaged numbers from technical duplicates or triplicates were used for statistics. Error bars indicate mean ± SEM; *p < 0.05, **p < 0.01. See also Figure S2.

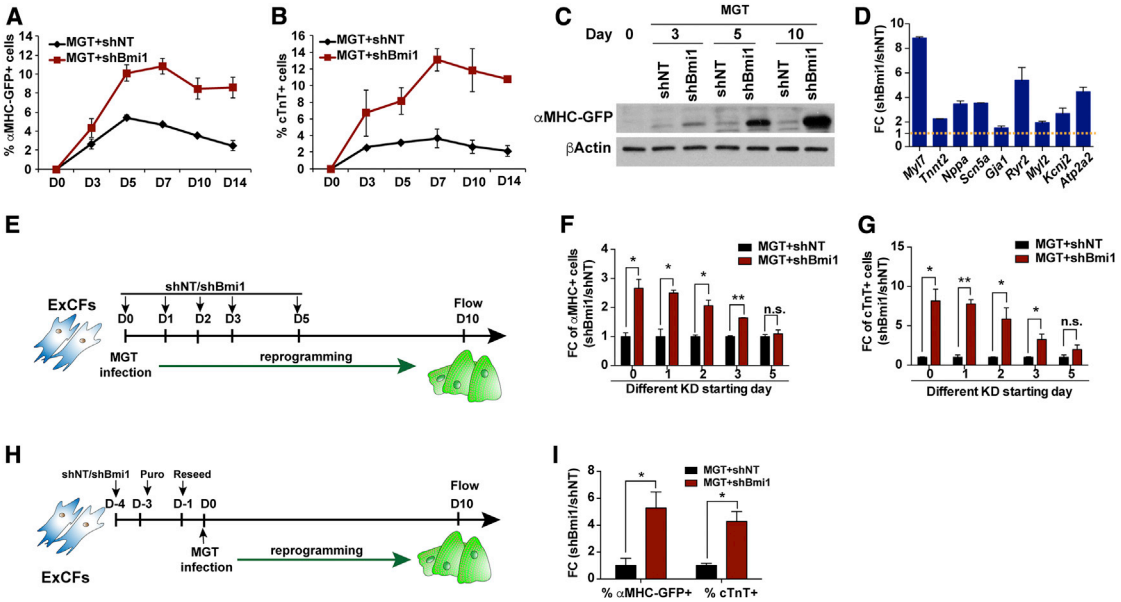

Figure 3. Bmi1 Functions during the Early Stage of iCM Reprogramming

(A and B) Histogram showing the percentages of αMHC-GFP+ cells (A) and cTnT+ cells (B) from flow analyses at indicated time points.

(C) Western blot of αMHC-GFP protein expression on ExCFs infected with MGT plus shNT or shBmi1 at indicated days. βActin was used as the loading control.

(D) Fold change (FC) in cardiac marker gene expression levels at reprogramming day 3 between MGT-transduced ExCFs infected with shBmi1 and the ones infected with shNT.

(E) Schematic of experimental design to determine the time window for *Bmi1* knockdown.

(F and G) Quantification of the fold change (FC) in the percentage of αMHC-GFP+ cells (F) and cTnT+ cells (G) reprogrammed as illustrated in (E). Values were normalized to the corresponding shNT control.

(H) Schematic of experimental design to determine the effect of knocking down *Bmi1* prior to MGT transduction.

(I) Quantification of the fold change (FC) in the percentage of αMHC-GFP+ and cTnT+ cells reprogrammed as illustrated in (H). Values were normalized to corresponding shNT control.

For each experiment, n = ~3–6; averaged numbers from technical duplicates or triplicates were used for statistics. Error bars indicate mean ± SEM; *p < 0.05, **p < 0.01.

percentages of αMHC-GPF+ and cTnT+ cells compared to those of the controls (Figure 3I). These data suggest that Bmi1 functions during the early stage of iCM reprogramming and that knockdown of *Bmi1* must occur within the first 3 days of or prior to MGT introduction to enhance iCM reprogramming.

Bmi1 Suppresses iCM Reprogramming Independent of Its Role in Regulating Cell Proliferation

One of the well-documented functions of Bmi1 is to regulate cell proliferation and senescence through its downstream effectors $p16^{Ink4a}$, $p19^{Arf}$, and p53 (Jacobs et al., 1999; Park et al., 2004). We asked if the enhancement of iCM reprogramming by *Bmi1* knockdown was mediated through an upregulation of $p16^{Ink4a}$ (isoform 2 of Cdkn2a), $p19^{Arf}$ (isoform 1 of Cdkn2a), or p53. We first analyzed their expression in control shNT- and shBmi1-infected reprogramming fibroblasts and found that *Bmi1* depletion indeed resulted in an upregulation of the expression of these target genes during iCM reprogramming (Figure S3A). We then knocked down *Bmi1* and its target genes simultaneously to determine if the increased reprogramming efficiency by *Bmi1* knockdown could be reversed by silencing Bmi1 target gene expression. qRT-PCR analysis indicated that we knocked down the expression of Bmi1 target genes by at least 90% (Figure S3B). Interestingly, quantification of flow cytometry analysis showed that the double knockdown cultures exhibited a significant increase in the percentages of αMHC-GPF+ and/or cTnT+ cells compared to the controls (Figure 4A), suggesting that the inhibitory effect of Bmi1 on iCM reprogramming was unlikely to be completely mediated by these downstream targets.

To further assess the effect of *p53* or $p19^{Arf}$ ablation on shBmi1-mediated enhancement of iCM reprogramming, we genetically ablated these genes by infecting neonatal ExCFs isolated from *p53* or $p19^{Arf}$ floxed mice with Ad-Cre-eGFP (Figures 4B–4E, S3C, and S3D). This approach allowed us to simultaneously excise the genes and label infected cells with eGFP. Ad-CMV-GFP infection was served as a control. qRT-PCR analysis revealed that *p53* or $p19^{Arf}$ expression in the Ad-Cre-eGFP infected fibroblasts was significantly reduced compared to that in the Ad-CMV-GFP infected ones (Figure S3C). These cells were then infected with MGT plus shBmi1 or shNT, and analysis of iCM markers was conducted on the GFP+ population of null or wild-type (fl/fl) control fibroblasts (Figure 4B). We observed that reprogramming efficiency of both *p53* null and control CFs was significantly increased by shBmi1 compared to shNT control (Figures 4C and 4D). Likewise, iCM reprogramming efficiency enhanced by *Bmi1* depletion was not suppressed by targeted deletion of $p19^{Arf}$ (Figure 4E). Interestingly, we found that the

expression of $p16^{Ink4a}$ increased when *p53* or $p19^{Arf}$ was knocked down and $p19^{Arf}$ was slightly upregulated upon *p53* or $p16^{Ink4a}$ depletion (Figure S3E), suggesting compensatory mechanisms between *p53*, $p16^{Ink4a}$, and $p19^{Arf}$. Therefore, we conducted double and triple knockdowns of *p53*, $p19^{Arf}$, and *Cdkn2*a to assess their roles in shBmi1-mediated enhancement of cardiac reprogramming. Flow cytometry analysis demonstrated that Bmi1-depleted cultures exhibited lower but still significant increases in the percentage of αMHC-GFP+ or cTnT+ cells compared to control cultures even when *Cdkn2a* and *p53* were simultaneously silenced (Figure 4F). To further determine if Bmi1 functions through these genes, we tested if overexpression of each could recapitulate the shBmi1 phenotype. Consistently, we found that overexpression of *p53*, $p16^{Ink4a}$, or $p19^{Arf}$ did not enhance and sometimes even lowered the percentages of αMHC-GFP+ or cTnT+ cells in MGT-transduced cultures (Figures S3F and S3G). Thus, the well-known downstream targets *p53*, $p16^{Ink4a}$, and $p19^{Arf}$ are unlikely to be the major downstream mediators of Bmi1 in cardiac reprogramming.

Based on previous reports that Bmi1 and its downstream targets are involved in cell proliferation and senescence (Jacobs et al., 1999; Levine, 1997; Quelle et al., 1995; Sharpless and DePinho, 1999), we sought to determine the requirement of cell proliferation in shBmi1-mediated iCM reprogramming. We used Mitomycin C (MMC), a commonly used inhibitor of cell proliferation, to block CF proliferation 2 days after MGT and shBmi1 or shNT transduction and examined the effect on shBmi1-mediated enhancement of iCM reprogramming (Figure 4G). Interestingly, although MMC treatment inhibited CF proliferation as evidenced by the lack of Ki67 staining in the nuclei of treated cells (Figure 4I), it did not have any noticeable effect on shBmi1-mediated enhancement of iCM reprogramming (Figures 4H and 4I). Next, we added MMC before the introduction of *Bmi1* shRNAs and treated the cells with 5-ethynyl-2′-deoxyuridine (EdU) to label the proliferating cells upon *Bmi1* knockdown (day 2 to day 10) or 2 days before assaying reprogramming efficiency (day 8 to day 10) (Figure 4J). Consistently, we found that almost all αMHC-GFP+ iCMs were EdU− in both shBmi1- and shNT-treated cultures (Figures 4K and 4L). The MMC treatment decreased the reprogramming efficiency; however, depleting *Bmi1* still resulted in an increased percentage of αMHC-GFP+ iCMs within EdU− cells when compared to the control, reflecting the effect of Bmi1 knockdown in non-proliferating fibroblasts (Figure 4M). These data suggest that Bmi1 functions to suppress iCM generation independently from its role in regulating its downstream effectors involved in cell proliferation.

Bmi1 Acts as a Repressor through Directly Binding to a Set of Cardiac Loci

As a key component of Polycomb Repressive Complex 1 (PRC1), Bmi1 is essential for PRC1 assembly and, together with the catalytic ring finger proteins Ring1A and Ring1B (Ring1A/B), mediates monoubiquitination of histone H2A at lysine 119 (H2AK119ub) to repress target gene expression (Cao et al., 2005; Ku et al., 2008; Morey et al., 2015). To gain insights into the mechanism by which Bmi1 modulates iCM reprogramming, we sought to identify direct targets of Bmi1. Interestingly, gene ontology analysis of recently published Bmi1 ChIP-seq data revealed an unexpected enrichment of key cardiac transcription factor genes (Gargiulo et al., 2013) (Figure S4A). This finding prompted us to perform further analysis of this Bmi1 ChIP-seq data as well as publically available global H3K4me3 and H3K27me3 genome mapping data generated with cardiac tissue or cardiac cells (Bernstein et al., 2012; Paige et al., 2012; Wamstad et al., 2012). Through this analysis, we identified strong Bmi1 binding peaks that overlapped with H3K4me3 or H3K27me3 occupied sites at the regulatory regions of cardiogenic genes, including *Gata4*, *Nkx2-5*, *Isl1*, *Pitx2*, *Tbx20*, *Hand2*, and *Smad6* (see reviews from Olson, 2006; Srivastava, 2006) (Figures 5A and S4B). We therefore postulated that Bmi1 repressed CM fate in non-myocytes by modulating chromatin accessibility of these key cardiac loci. To test this hypothesis, we performed Bmi1 ChIP assay followed by qPCR on MEFs to quantify the enrichment of Bmi1-bound DNA fragments from these cardiogenic gene loci (Figures 5B and S4C). Indeed, we found that Bmi1 bound at distinct regions of the cardiac loci *Gata4*, *Nkx2.5*, *Isl1*, *Pitx2*, *Tbx20*, and *Hand2*, but not *Smad6*, in fibroblasts. For instance, Bmi1 bound to *Gata4* locus primarily at G3, approximately −3136 to −3029 base pairs (bp) upstream from the transcription start site (TSS); Bmi1 bound to *Nkx2.5* locus primarily at N6 from −9360 to −9229 bp relative to TSS, which contains Gata factor binding sites and less at N3 from −5842 to −5665 bp relative to TSS where Smad factors bind (Figures 5A and 5B). ChIP-qPCR experiments also revealed that the Bmi1-bound cardiac loci were co-occupied by H2AK119ub, Ring1B, and the PRC2 key component Ezh2 (Figures 5C–5E), suggesting a repressive chromatin state of these cardiac loci in fibroblasts.

To test if Bmi1 modulated chromatin status of the cardiogenic genes during the early stage of reprogramming, we performed ChIP-qPCR of H2AK119ub, H3K4me3, and H3K27me3 on *Bmi1*-depleted and control MEFs that had been transduced with MGT for 3 days. The positive and negative controls for ChIP-qPCR of each mark are shown in Figure S4D. Upon Bmi1 depletion, H2AK119ub at the cardiogenic loci was completely removed (Figures 5F and S4E), consistent with Bmi1's role in PRC1 assembly to promote monoubiquitination of H2AK119. Additionally, in the absence of Bmi1, H3K4me3 levels were moderately increased at the regulatory regions of *Gata4*, *Isl1*, *Pitx2*, and *Tbx20* near where Bmi1 binds (Figures 5G and S4E). Interestingly, the most significant enhancement of H3K4me3 level was detected at the *Gata4* locus (Figure 5G). In contrast, H3K27me3 modifications at the same loci were barely affected by *Bmi1* knockdown (Figures 5H and S4E). We only detected a decrease in H3K27me3 modification in the P2 region of *Pitx2* and T3 region of *Tbx20* (Figure 5H). The *Smad6* locus that was not bound by Bmi1 exhibited low levels of H2AK119ub and H3K27me3. In addition, H3K4me3 levels at *Smad6* were unaltered by loss of Bmi1 (Figures S4D and S4E, lower panel). Consistent with the increase in the level of H3K4me3 and a major loss of H2AK119ub at the loci, the endogenous mRNA expression of *Gata4*, *Isl1*, *Pitx2*, and *Tbx20* was significantly upregulated by *Bmi1* knockdown during iCM reprogramming (Figures 5I). In contrast, *Bmi1* knockdown did not affect the expression levels of the genes (*Nkx2-5* and *Hand2*) whose loci exhibited reduced H2AK119ub, but unaltered H3K4me3 levels (Figures 5I, S4E, and S4G). These data suggest that removal of the repressive mark H2AK119ub is not sufficient to induce the

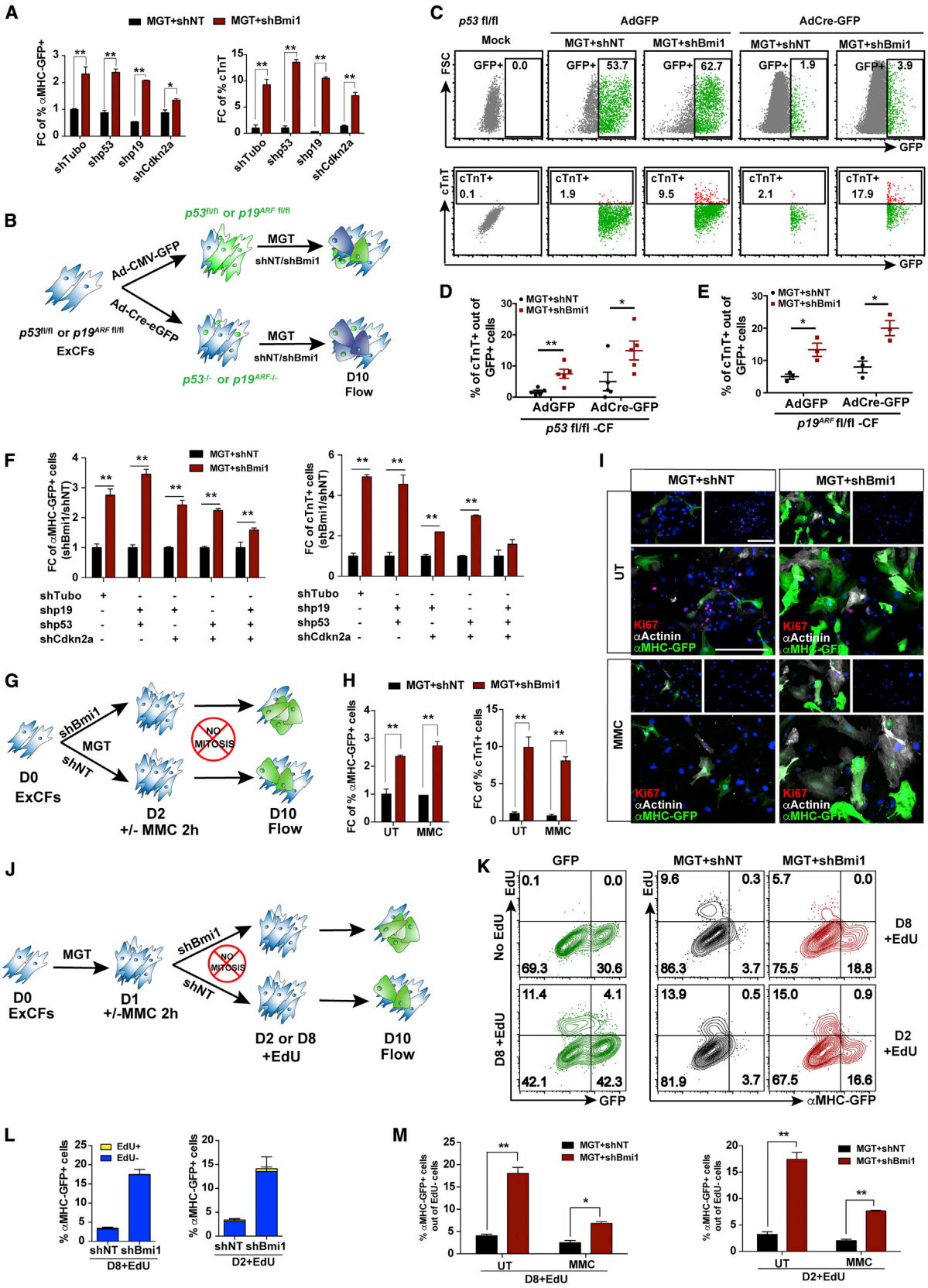

(legend on next page)

expression of all the Bmi1-bound cardiogenic genes. The increase in the level of H3K4me3 in addition to a loss of H2AK119ub, however, is more closely correlated with de-repression of cardiogenic gene expression.

In order to determine if Bmi1 only repressed the expression of the cardiogenic genes during iCM reprogramming, we re-analyzed the ChIP-seq data (Bernstein et al., 2012; Gargiulo et al., 2013; Paige et al., 2012; Wamstad et al., 2012) and identified Bmi1 binding peaks that were overlapped with H3K27me3 and H3K4me3 binding sites at other lineage loci (Figure S4H). We carefully selected representative loci encoding regulators of other lineages, including *Zic1* and *Sox2* (neuron), *Pax2* and *Sall1* (kidney), and *Nkx6-1* and *Sox9* (pancreas) to determine the regulation by Bmi1 during iCM reprogramming (Figure S4H). We found that only two loci (*Pax2* and *Nkx6-1*) had Bmi1 binding peaks that overlapped with H2AK119ub, Ring1B, and Ezh2 binding sites and upregulated their expression upon *Bmi1* knockdown (Figures S4H–S4K). However, Bmi1 knockdown did not have any noticeable effect on gene expression of other loci (Figure S4I).

Taken together, our data suggest that Bmi1 regulates a set of critical cardiogenic factors through directly binding to their regulatory regions to modulate their chromatin status and expression.

iCM Reprogramming using Two Transcription Factors, Mef2c and Tbx5

We were intrigued to find that among the identified targets of Bmi1, Gata4, one of the transcription factors used for iCM reprogramming (Addis et al., 2013; Fu et al., 2013; Ieda et al., 2010; Ifkovits et al., 2014; Inagawa et al., 2012; Nam et al., 2013; Qian et al., 2012; Song et al., 2012), was most significantly upregulated in *Bmi1*-depleted fibroblasts (Figure 5I). Moreover, Gata4 can function as a pioneer transcription factor that binds to its target sites on nucleosomes or compacted chromatin (Cirillo et al., 2002). Because removing Bmi1 de-repressed endogenous *Gata4* and other cardiogenic genes, we postulated that *Bmi1* depletion could replace Gata4 in reprogramming fibroblasts into functional iCMs. We systematically evaluated all possible two or one cardiac reprogramming factor combinations for their capacity to reprogram shNT or shBmi1 fibroblasts into iCMs. Flow cytometry analysis revealed that only Mef2c in combination with Tbx5 (M+T) efficiently converted shBmi1, but not the shNT control, fibroblasts into iCMs that expressed CM marker gene expression (Figure 6A).

Next, to determine if iCM generation could be achieved with a single vector, we generated two polycistronic constructs to express *Mef2c* and *Tbx5* in a single mRNA (MT and TM, Figure 6B). The construct with Mef2c at the first position resulted in a higher reprogramming efficiency than the other (Figures 6C and 6D), consistent with our previous finding that stoichiometry of the reprogramming factors influences iCM reprogramming (Wang et al., 2015a). Moreover, the capability of MT plus shBmi1 to reprogram fibroblasts into αMHC-GFP+ and/or cTnT+ cells was abolished upon the depletion of *Gata4* (Figures 6E, S5A, and S5B), suggesting that Gata4 was one of the major downstream effectors of Bmi1 during iCM reprogramming. Importantly, iCMs generated by MT overexpression with *Bmi1* knockdown not only turned on cardiac marker gene expression, but also assembled sarcomere structures and exhibited calcium oscillation and spontaneous contraction after 2–4 weeks of culture (Figures 6F–6H, Movie S4, and Movie S5), while none of these features were observed with shNT and MT co-infected fibroblasts. Taken together, our results demonstrate that, after removing epigenetic barriers by Bmi1 depletion, Mef2c and Tbx5 are sufficient to reprogram fibroblasts into functional beating iCMs.

DISCUSSION

In this study, we performed a functional screen to identify epigenetic regulators of direct cardiac reprogramming. Knocking down a selected set of epigenetic modulators either increased or reduced iCM reprogramming efficiency, highlighting the importance of epigenetic regulation in iCM reprogramming. Specifically, we found that Bmi1 functioned as a major epigenetic barrier at the early stage of iCM reprogramming. Through a series of epistatic analyses, we demonstrated that the effect of silencing *Bmi1* on cardiac reprogramming was unlikely mediated by its known targets $p16^{Ink4a}$, $p19^{Arf}$, or *p53*. In an effort to explore the underlying mechanism, we found that Bmi1 directly bound to a set of key cardiogenic loci that are co-occupied by other PRC components. Knockdown of Bmi1 resulted in a major loss of H2AK119ub and an increase in H3K4me3 levels at these

Figure 4. Bmi1 Suppresses iCM Reprogramming Independent of Cell Proliferation

(A) Quantification of the fold change (FC) in the percentage of the αMHC-GFP+ and cTnT+ cells reprogrammed with indicated shRNAs at day 10. shTubo was used as additional non-targeting control. Values were normalized to the controls.

(B–E) Experiments to determine the effect of targeted deletion of *p53* or $p19^{ARF}$ on shBmi1-enhanced iCM reprogramming using genetic floxed mice, with schematic in (B), and representative flow plots and quantification in (C)–(E).

(F) Quantification of the fold change (FC) in the percentage of αMHC-GFP+ and cTnT+ cells reprogrammed with indicated shRNA combinations at day 10. Values were normalized to the corresponding shNT control.

(G–I) Experiments to determine the effect of Mitomycin C (MMC) treatment on shBmi1-mediated enhancement of iCM reprogramming, with schematic in (G), quantification of flow analyses in (H), and representative ICC pictures of αActinin (white), αMHC-GFP (green), and Ki67 (magenta) in (I). DAPI (blue) indicated nuclei. Scale bars, 200 μm.

(J–M) The effect of cell proliferation on shBmi1-mediated enhancement of iCM reprogramming. (J) Schematic of the EdU incorporation experiment. (K and L) Representative flow contour plots and quantification without MMC treatment. (M) Quantification of flow analysis for the percentage of αMHC-GFP+ cells out of EdU− cells upon MMC treatment. The starting time point for EdU incorporation is indicated. GFP transduced cells with or without EdU treatment were used as gating controls. UT stands for EdU untreated culture.

For each experiment, n = ~3–6; averaged numbers from technical duplicates or triplicates were used for statistics. For (D) and (E), each dot represents one experiment from one litter of pups. Error bars indicate mean ± SEM; *$p < 0.05$, **$p < 0.01$. See also Figure S3.

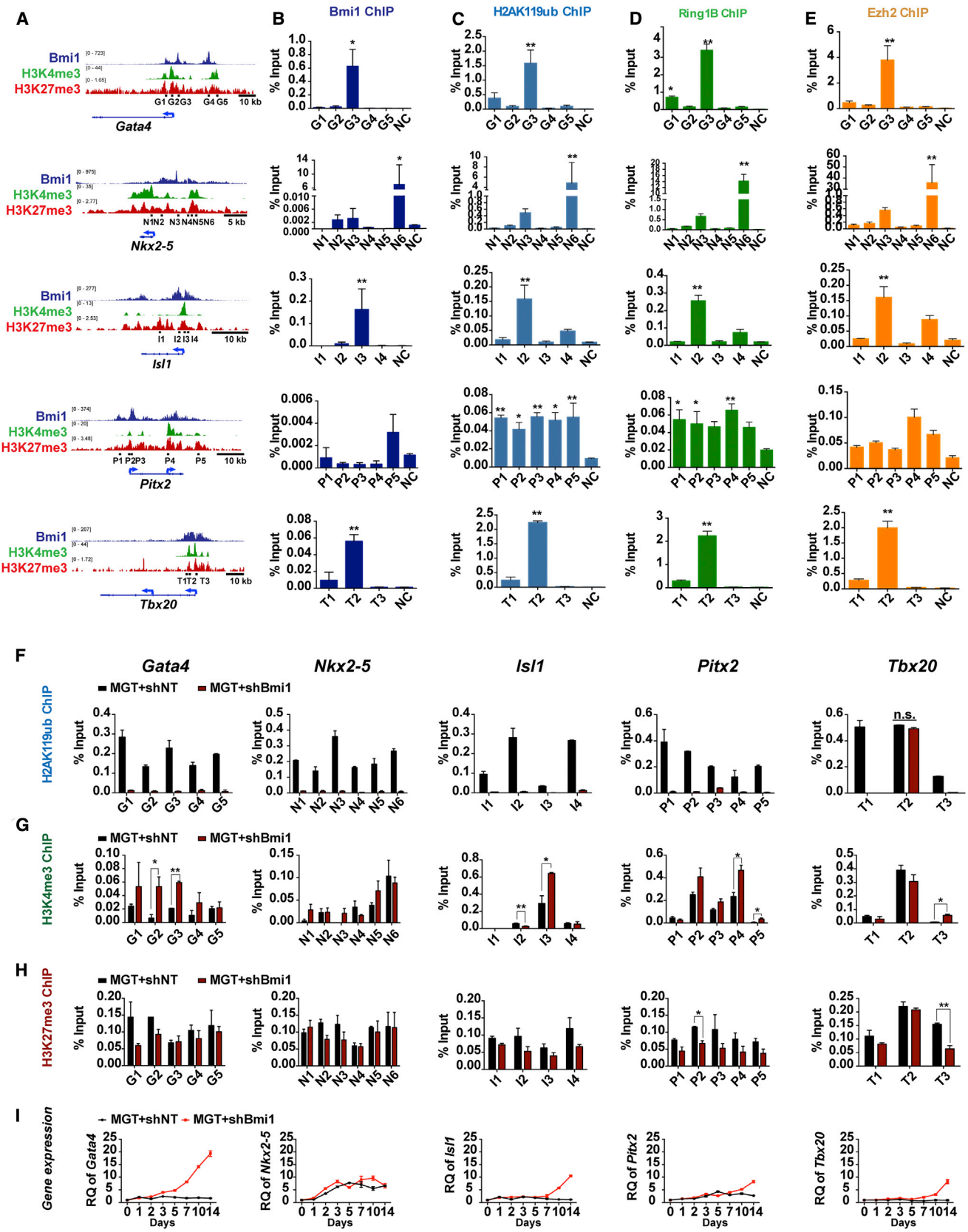

(legend on next page)

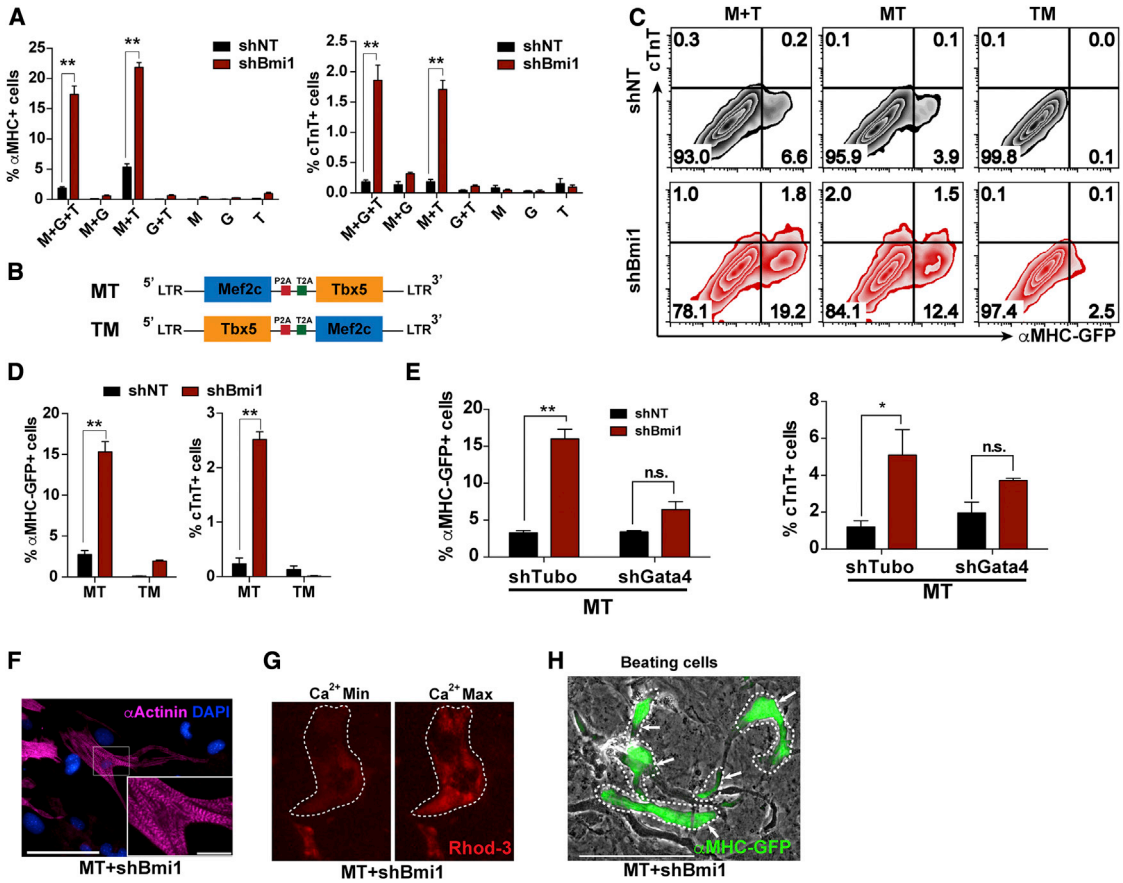

Figure 6. Mef2c and Tbx5 Reprogrammed Bmi1-Depleted Fibroblasts into iCMs

(A) Quantification of flow analyses for αMHC-GFP+ or cTnT+ cells on shNT- or shBmi1-infected ExCFs expressing different combinations of Mef2c, Gata4, and Tbx5.

(B) Schematics of the two bicistronic vectors encoding Mef2c and Tbx5 in different splicing orders.

(C) Representative flow contour plots of αMHC-GFP+ and cTnT+ cells derived from shNT- or shBmi1-infected ExCFs expressing Mef2c and Tbx5 as indicated.

(D) Quantification of flow data in (C).

(E) Quantification of flow analyses for αMHC-GFP+ (left) and cTnT+ (right) cells on MT-transduced ExCFs co-infected with shRNA targeting *Bmi1*, *Gata4*, or non-targeting control shNT or shTubo as indicated.

(F) Representative ICC image of iCMs labeled by αActinin reprogrammed using MT and shBmi1 at day 14. Inset is a high-magnification image of the area highlighted by white rectangle. Left, scale bar, 100 μm; inset, scale bar, 20 μm.

(G) Representative calcium transients in iCM labeled with Rhod-3 4 weeks after MT and shBmi1 transduction on freshly isolated CFs, corresponding to Movie S4.

(H) Representative αMHC-GFP+ beating cells (highlighted by white arrows and white dash lines) derived from MT and shBmi1 co-infected fresh CFs 4 weeks after viral transduction. The corresponding movie is shown in Movie S5. Scale bar, 100 μm.

Data in (A–E) were collected on reprogramming day 10. For each experiment, n = ~3–6; averaged numbers from technical duplicates were used for statistics. Error bars indicate mean ± SEM; *p < 0.05, **p < 0.01. n.s., not significant. See also Figure S5.

cardiac loci and de-repression of cardiogenic gene expression. This is consistent with previously published findings that H2AK119 monoubiquitination by PRC1 is associated with gene repression (Cao et al., 2005; Wang et al., 2004). It is also possible that knockdown of *Bmi1* de-compacted chromatin and increased DNA accessibility (Abdouh et al., 2016; Eskeland et al., 2010; Francis et al., 2004; Levine et al., 2002; Shao et al., 1999), thereby de-repressing *Gata4* and the other

Figure 5. Bmi1 Knockdown Resulted in Acquisition of Active Chromatin Status at the Cardiac Loci

(A) The density of Bmi1, H3K4me3, and H3K27me3 ChIP-seq reads at the indicated gene loci. The gene name initial followed by numbers denotes a series of amplicons that correspond to the binding sites.

(B–E) ChIP-qPCR for Bmi1 (B), H2AK119ub (C), Ring1B (D), or Ezh2 (E) on MEFs at indicated cardiac gene loci. NC (unrelated genomic locus ~22 kb upstream to the TSS of *Pitx2* gene) was used as a negative control.

(F–H) ChIP-qPCR for H2AK119ub (F), H3K4me3 (G), and H3K27me3 (H) at cardiac gene loci on MEFs 3 days after transduction of MGT and shRNA targeting *Bmi1* or control.

(I) qRT-PCR of endogenous cardiac gene expression on shNT or shBmi1-infected MGT-expressing MEFs at different time points. Expression at reprogramming day 0 was set as 1. RQ stands for relative quantification.

For each experiment, n = ~3–6; averaged numbers from technical duplicates were used for statistics. Error bars indicate mean ± SEM; *p < 0.05, **p < 0.01. n.s., not significant. See also Figure S4.

cardiogenic genes. Interestingly, this de-repression of endogenous *Gata4* by *Bmi1* depletion could substitute for exogenous Gata4 in reprogramming fibroblasts into beating iCMs, demonstrating that removing certain epigenetic barriers could allow efficient iCM generation with fewer transcription factors.

To the best of our knowledge, the screen we performed in this study represents the first loss-of-function screen to study the role of chromatin-associated proteins in iCM reprogramming. Although our shRNA-based screen was not genome-wide, and nor does it cover all epigenetic factors, this study provides proof-of-concept evidence demonstrating the feasibility of an RNAi-mediated functional screen to identify key epigenetic barriers to iCM reprogramming. Given the functional conservation of many epigenetic regulators, especially Bmi1 (98% identity at protein level), between mouse and human, it is likely that removing similar epigenetic barriers in human fibroblasts will lead to improved generation of human iCMs for clinical studies. Furthermore, the platform and conditions described in this study could be leveraged to develop high-throughput large-scale loss-of-function screens. In combination with other approaches such as single-cell omics, it will be possible in the near future to identify each barrier during iCM reprogramming and to leverage this knowledge to alleviate the roadblocks to enhance and accelerate iCM reprogramming.

In addition to Bmi1, we identified a set of epigenetic factors that function as facilitators of or barriers to cardiac reprogramming. These results will stimulate follow-up studies to further interrogate the role of epigenetic factors in iCM reprogramming. Of particular note is the finding that knocking down three MYST histone acetyltransferase family members moderately promoted iCM reprogramming (Figure 1C and Table S1), highlighting the importance of histone acetylation in iCM reprogramming. This finding also suggests possible functional redundancy and compensation among members of epigenetic regulators that belong to the same family. While knocking down *Plu1* enhanced iPSC reprogramming (Kidder et al., 2013), silencing *Plu1* remarkably reduced iCM reprogramming efficiency (Figures 1B, Table S1). Likewise, we observed an opposite effect of *Bmi1* knockdown on iCM versus iPSC reprogramming efficiency and transdifferentiation of neural stem cells (Moon et al., 2011; Onder et al., 2012). Meanwhile, silencing the *Ink4a/Arf* locus, the well-known downstream target repressed by Bmi1 that functions as a barrier to iPSC and neuronal reprogramming (Li et al., 2009; Price et al., 2014), did not exhibit any noticeable effect on cardiac reprogramming. Our work thus suggests that direct lineage reprogramming, or at least iCM reprogramming, might employ distinct epigenetic regulatory mechanisms from iPSC reprogramming to directly convert one somatic cell type to another.

EXPERIMENTAL PROCEDURES

Primary Cell Cultures

Hearts and tail-tips from neonatal pups (day 1.5) or adult mice (4 weeks) were isolated for explant culture. After 7 days, explant cells were separated by magnetic cell sorting (MACS) so we could obtain Thy1.2+ neonatal or adult CFs and TTFs. CD31+ endothelial cells were derived from explant culture of neonatal hearts by MACS. Fresh CFs were derived from neonatal hearts and underwent MACS via anti-Thy1.2 antibody (Miltenyi Biotec) as described previously (Wang et al., 2015a, 2015b). MEFs were prepared as previously described (Jozefczuk et al., 2012). Detailed descriptions of the isolation of each cell type are available in the Supplemental Information.

Viral Packaging and Direct Reprogramming

The protocol of viral packaging is as described in the Supplemental Information. To generate iCMs, fibroblasts or CD31+ endothelial cells were transduced with MGT retroviruses and lentiviruses expressing shRNAs in iCM media (10% FBS of DMEM/M199 [4:1]). At the indicated time points, reprogramming cells were harvested for analyses. For the beating assay, freshly isolated CFs were used. After viral infection and 10 days of culture in iCM media, cells were changed into StemPro-34 SF medium (SPF34, GIBCO) supplemented with GlutaMAX (GIBCO), Ascorbic acid (Sigma), VEGF, bFGF, and FGF10 (all from R & D Systems). Four to six weeks after viral infection, the number of spontaneously beating cells was counted under an EVOS microscope (40×). Detailed protocols of iCM and iN generation are available in the Supplemental Information.

Flow Cytometry and ICC

Flow cytometry analysis and ICC were performed as previously described (Wang et al., 2015a, 2015b). The experimental procedure and antibody information are available in the Supplemental Information.

qPCR, ChIP, and Western Blot

Total RNA was isolated with TRIzol (Invitrogen) and reverse-transcribed into cDNA using SuperScript III Reverse Transcriptase (Invitrogen). qRT-PCR was performed using the ABI ViiA 7 Real-Time PCR system (Applied Biosystems) and the Power SYBR Green PCR Master Mix (Applied Biosystems) or Taqman Gene Expression Master Mix (Taqman, ABI) according to the manufacturer's instructions. The primer sequences and Taqman probes used for qRT-PCR are provided in Table S2. ChIP was performed on MEFs according to a previously described protocol (Cai et al., 2013) with minor modification as described in the Supplemental Information. Western blots were performed as described previously (Wang et al., 2015a). Antibody information is available in the Supplemental Information.

SUPPLEMENTAL INFORMATION

Supplemental Information for this article includes five figures, two tables, five movies, and Supplemental Experimental Procedures and can be found with this article online at http://dx.doi.org/10.1016/j.stem.2016.02.003.

AUTHOR CONTRIBUTIONS

Y.Z. designed and performed experiments, analyzed data, and wrote the manuscript. L.W. designed and performed experiments and analyzed data. H.R.V. performed experiments, analyzed data, and wrote the manuscript. Z.L., S.A., and C.Y. performed experiments and commented on the manuscript. R.L., J.-D.F., and G.G.W. provided critical reagents and comments on the manuscript. J.L. supervised the work and wrote the manuscript. L.Q. supervised the work, designed the experiments, analyzed data, and wrote the manuscript.

ACKNOWLEDGMENTS

We are grateful for the expert technical assistance from the UNC Flow Cytometry Core and UNC Microscopy Core. We thank members of the Qian and Liu laboratories and Drs. V. Bautch, J. Taylor, and C. Mack for helpful discussions and critical reviews of the manuscript. H.R.V. is supported by an NIH T32 training grant HL069768-14 (PI, Nobuyo Maeda) and a UNC Pathology Sylke Scholarship. R.L. is supported by a postdoc fellowship from Lymphoma Research Foundation. This study was supported by American Heart Association (AHA) Scientist Development Grant 13SDG14580035 to J.D.F., NCI R00 Award CA151683 to G.G.W. (G.G.W. is a Kimmel Scholar of Sidney Kimmel Foundation for Cancer Research), NIH/NHLBI R00 HL109079 grant to J.L., and American Heart Association (AHA) Scientist Development Grant 13SDG17060010 and the Ellison Medical Foundation (EMF) New Scholar Grant AG-NS-1064-13 to L.Q.

Received: June 1, 2015
Revised: November 1, 2015
Accepted: February 12, 2016
Published: March 3, 2016

REFERENCES

Abdouh, M., Hanna, R., El Hajjar, J., Flamier, A., and Bernier, G. (2016). The Polycomb Repressive Complex 1 Protein BMI1 Is Required for Constitutive Heterochromatin Formation and Silencing in Mammalian Somatic Cells. J. Biol. Chem. *291*, 182–197.

Addis, R.C., and Epstein, J.A. (2013). Induced regeneration–the progress and promise of direct reprogramming for heart repair. Nat. Med. *19*, 829–836.

Addis, R.C., Ifkovits, J.L., Pinto, F., Kellam, L.D., Esteso, P., Rentschler, S., Christoforou, N., Epstein, J.A., and Gearhart, J.D. (2013). Optimization of direct fibroblast reprogramming to cardiomyocytes using calcium activity as a functional measure of success. J. Mol. Cell. Cardiol. *60*, 97–106.

Apostolou, E., and Hochedlinger, K. (2013). Chromatin dynamics during cellular reprogramming. Nature *502*, 462–471.

Bernstein, B.E., Birney, E., Dunham, I., Green, E.D., Gunter, C., and Snyder, M.; ENCODE Project Consortium (2012). An integrated encyclopedia of DNA elements in the human genome. Nature *489*, 57–74.

Buganim, Y., Faddah, D.A., and Jaenisch, R. (2013). Mechanisms and models of somatic cell reprogramming. Nat. Rev. Genet. *14*, 427–439.

Cai, L., Rothbart, S.B., Lu, R., Xu, B., Chen, W.-Y., Tripathy, A., Rockowitz, S., Zheng, D., Patel, D.J., Allis, C.D., et al. (2013). An H3K36 methylation-engaging Tudor motif of polycomb-like proteins mediates PRC2 complex targeting. Mol. Cell *49*, 571–582.

Cao, R., Tsukada, Y., and Zhang, Y. (2005). Role of Bmi-1 and Ring1A in H2A ubiquitylation and Hox gene silencing. Mol. Cell *20*, 845–854.

Chen, J.X., Krane, M., Deutsch, M.A., Wang, L., Rav-Acha, M., Gregoire, S., Engels, M.C., Rajarajan, K., Karra, R., Abel, E.D., et al. (2012). Inefficient reprogramming of fibroblasts into cardiomyocytes using Gata4, Mef2c, and Tbx5. Circ. Res. *111*, 50–55.

Cirillo, L.A., Lin, F.R., Cuesta, I., Friedman, D., Jarnik, M., and Zaret, K.S. (2002). Opening of compacted chromatin by early developmental transcription factors HNF3 (FoxA) and GATA-4. Mol. Cell *9*, 279–289.

Dhawan, S., Georgia, S., Tschen, S.I., Fan, G., and Bhushan, A. (2011). Pancreatic β cell identity is maintained by DNA methylation-mediated repression of Arx. Dev. Cell *20*, 419–429.

Eskeland, R., Leeb, M., Grimes, G.R., Kress, C., Boyle, S., Sproul, D., Gilbert, N., Fan, Y., Skoultchi, A.I., Wutz, A., and Bickmore, W.A. (2010). Ring1B compacts chromatin structure and represses gene expression independent of histone ubiquitination. Mol. Cell *38*, 452–464.

Francis, N.J., Kingston, R.E., and Woodcock, C.L. (2004). Chromatin compaction by a polycomb group protein complex. Science *306*, 1574–1577.

Fu, J.D., Stone, N.R., Liu, L., Spencer, C.I., Qian, L., Hayashi, Y., Delgado-Olguin, P., Ding, S., Bruneau, B.G., and Srivastava, D. (2013). Direct reprogramming of human fibroblasts toward a cardiomyocyte-like state. Stem Cell Reports *1*, 235–247.

Gargiulo, G., Cesaroni, M., Serresi, M., de Vries, N., Hulsman, D., Bruggeman, S.W., Lancini, C., and van Lohuizen, M. (2013). In vivo RNAi screen for BMI1 targets identifies TGF-β/BMP-ER stress pathways as key regulators of neural- and malignant glioma-stem cell homeostasis. Cancer Cell *23*, 660–676.

Geiman, T.M., Tessarollo, L., Anver, M.R., Kopp, J.B., Ward, J.M., and Muegge, K. (2001). Lsh, a SNF2 family member, is required for normal murine development. Biochim. Biophys. Acta *1526*, 211–220.

Hirai, H., Katoku-Kikyo, N., Keirstead, S.A., and Kikyo, N. (2013). Accelerated direct reprogramming of fibroblasts into cardiomyocyte-like cells with the MyoD transactivation domain. Cardiovasc. Res. *100*, 105–113.

Ieda, M., Fu, J.D., Delgado-Olguin, P., Vedantham, V., Hayashi, Y., Bruneau, B.G., and Srivastava, D. (2010). Direct reprogramming of fibroblasts into functional cardiomyocytes by defined factors. Cell *142*, 375–386.

Ifkovits, J.L., Addis, R.C., Epstein, J.A., and Gearhart, J.D. (2014). Inhibition of TGFβ signaling increases direct conversion of fibroblasts to induced cardiomyocytes. PLoS ONE *9*, e89678.

Inagawa, K., Miyamoto, K., Yamakawa, H., Muraoka, N., Sadahiro, T., Umei, T., Wada, R., Katsumata, Y., Kaneda, R., Nakade, K., et al. (2012). Induction of cardiomyocyte-like cells in infarct hearts by gene transfer of Gata4, Mef2c, and Tbx5. Circ. Res. *111*, 1147–1156.

Jacobs, J.J., Kieboom, K., Marino, S., DePinho, R.A., and van Lohuizen, M. (1999). The oncogene and Polycomb-group gene bmi-1 regulates cell proliferation and senescence through the ink4a locus. Nature *397*, 164–168.

Jayawardena, T.M., Egemnazarov, B., Finch, E.A., Zhang, L., Payne, J.A., Pandya, K., Zhang, Z., Rosenberg, P., Mirotsou, M., and Dzau, V.J. (2012). MicroRNA-mediated in vitro and in vivo direct reprogramming of cardiac fibroblasts to cardiomyocytes. Circ. Res. *110*, 1465–1473.

Jozefczuk, J., Drews, K., and Adjaye, J. (2012). Preparation of Mouse Embryonic Fibroblast Cells Suitable for Culturing Human Embryonic and Induced Pluripotent Stem Cells. J. Vis. Exp. *64*, http://dx.doi.org/10.3791/3854.

Kidder, B.L., Hu, G., Yu, Z.-X., Liu, C., and Zhao, K. (2013). Extended self-renewal and accelerated reprogramming in the absence of Kdm5b. Mol. Cell. Biol. *33*, 4793–4810.

Ku, M., Koche, R.P., Rheinbay, E., Mendenhall, E.M., Endoh, M., Mikkelsen, T.S., Presser, A., Nusbaum, C., Xie, X., Chi, A.S., et al. (2008). Genomewide analysis of PRC1 and PRC2 occupancy identifies two classes of bivalent domains. PLoS Genet. *4*, e1000242.

Laflamme, M.A., and Murry, C.E. (2011). Heart regeneration. Nature *473*, 326–335.

Levine, A.J. (1997). p53, the cellular gatekeeper for growth and division. Cell *88*, 323–331.

Levine, S.S., Weiss, A., Erdjument-Bromage, H., Shao, Z., Tempst, P., and Kingston, R.E. (2002). The core of the polycomb repressive complex is compositionally and functionally conserved in flies and humans. Mol. Cell. Biol. *22*, 6070–6078.

Li, H., Collado, M., Villasante, A., Strati, K., Ortega, S., Can, M., Blasco, M.A., and Serrano, M. (2009). The Ink4/Arf locus is a barrier for iPS cell reprogramming. Nature *460*, 1136–1139.

Liang, G., and Zhang, Y. (2013). Embryonic stem cell and induced pluripotent stem cell: an epigenetic perspective. Cell Res. *23*, 49–69.

Luna-Zurita, L., and Bruneau, B.G. (2013). Chromatin modulators as facilitating factors in cellular reprogramming. Curr. Opin. Genet. Dev. *23*, 556–561.

Moon, J.-H., Heo, J.S., Kim, J.S., Jun, E.K., Lee, J.H., Kim, A., Kim, J., Whang, K.Y., Kang, Y.-K., Yeo, S., et al. (2011). Reprogramming fibroblasts into induced pluripotent stem cells with Bmi1. Cell Res. *21*, 1305–1315.

Morey, L., Santanach, A., Blanco, E., Aloia, L., Nora, E.P., Bruneau, B.G., and Di Croce, L. (2015). Polycomb Regulates Mesoderm Cell Fate-Specification in Embryonic Stem Cells through Activation and Repression Mechanisms. Cell Stem Cell *17*, 300–315.

Muraoka, N., Yamakawa, H., Miyamoto, K., Sadahiro, T., Umei, T., Isomi, M., Nakashima, H., Akiyama, M., Wada, R., Inagawa, K., et al. (2014). MiR-133 promotes cardiac reprogramming by directly repressing Snai1 and silencing fibroblast signatures. EMBO J. *33*, 1565–1581.

Nam, Y.-J., Song, K., Luo, X., Daniel, E., Lambeth, K., West, K., Hill, J.A., DiMaio, J.M., Baker, L.A., Bassel-Duby, R., and Olson, E.N. (2013). Reprogramming of human fibroblasts toward a cardiac fate. Proc. Natl. Acad. Sci. USA *110*, 5588–5593.

Olson, E.N. (2006). Gene regulatory networks in the evolution and development of the heart. Science *313*, 1922–1927.

Onder, T.T., Kara, N., Cherry, A., Sinha, A.U., Zhu, N., Bernt, K.M., Cahan, P., Marcarci, B.O., Unternaehrer, J., Gupta, P.B., et al. (2012). Chromatin-modifying enzymes as modulators of reprogramming. Nature *483*, 598–602.

Paige, S.L., Thomas, S., Stoick-Cooper, C.L., Wang, H., Maves, L., Sandstrom, R., Pabon, L., Reinecke, H., Pratt, G., Keller, G., et al. (2012). A temporal chromatin signature in human embryonic stem cells identifies regulators of cardiac development. Cell *151*, 221–232.

Papp, B., and Plath, K. (2013). Epigenetics of reprogramming to induced pluripotency. Cell *152*, 1324–1343.

Park, I.K., Morrison, S.J., and Clarke, M.F. (2004). Bmi1, stem cells, and senescence regulation. J. Clin. Invest. *113*, 175–179.

Porrello, E.R., Mahmoud, A.I., Simpson, E., Hill, J.A., Richardson, J.A., Olson, E.N., and Sadek, H.A. (2011). Transient Regenerative Potential of the Neonatal Mouse Heart. Science *331*, 1078–1080.

Price, J.D., Park, K.-Y., Chen, J., Salinas, R.D., Cho, M.J., Kriegstein, A.R., and Lim, D.A. (2014). The Ink4a/Arf locus is a barrier to direct neuronal transdifferentiation. J. Neurosci. *34*, 12560–12567.

Protze, S., Khattak, S., Poulet, C., Lindemann, D., Tanaka, E.M., and Ravens, U. (2012). A new approach to transcription factor screening for reprogramming of fibroblasts to cardiomyocyte-like cells. J. Mol. Cell. Cardiol. *53*, 323–332.

Qian, L., and Srivastava, D. (2013). Direct cardiac reprogramming: from developmental biology to cardiac regeneration. Circ. Res. *113*, 915–921.

Qian, L., Huang, Y., Spencer, C.I., Foley, A., Vedantham, V., Liu, L., Conway, S.J., Fu, J.D., and Srivastava, D. (2012). In vivo reprogramming of murine cardiac fibroblasts into induced cardiomyocytes. Nature *485*, 593–598.

Qian, L., Berry, E.C., Fu, J.D., Ieda, M., and Srivastava, D. (2013). Reprogramming of mouse fibroblasts into cardiomyocyte-like cells in vitro. Nat. Protoc. *8*, 1204–1215.

Quelle, D.E., Zindy, F., Ashmun, R.A., and Sherr, C.J. (1995). Alternative reading frames of the INK4a tumor suppressor gene encode two unrelated proteins capable of inducing cell cycle arrest. Cell *83*, 993–1000.

Shao, Z., Raible, F., Mollaaghababa, R., Guyon, J.R., Wu, C.T., Bender, W., and Kingston, R.E. (1999). Stabilization of chromatin structure by PRC1, a Polycomb complex. Cell *98*, 37–46.

Sharpless, N.E., and DePinho, R.A. (1999). The INK4A/ARF locus and its two gene products. Curr. Opin. Genet. Dev. *9*, 22–30.

Song, K., Nam, Y.-J., Luo, X., Qi, X., Tan, W., Huang, G.N., Acharya, A., Smith, C.L., Tallquist, M.D., Neilson, E.G., et al. (2012). Heart repair by reprogramming non-myocytes with cardiac transcription factors. Nature *485*, 599–604.

Srivastava, D. (2006). Making or breaking the heart: from lineage determination to morphogenesis. Cell *126*, 1037–1048.

Tursun, B., Patel, T., Kratsios, P., and Hobert, O. (2011). Direct conversion of C. elegans germ cells into specific neuron types. Science *331*, 304–308.

Ubil, E., Duan, J., Pillai, I.C.L., Rosa-Garrido, M., Wu, Y., Bargiacchi, F., Lu, Y., Stanbouly, S., Huang, J., Rojas, M., et al. (2014). Mesenchymal-endothelial transition contributes to cardiac neovascularization. Nature *514*, 585–590.

van der Lugt, N.M.T., Domen, J., Linders, K., van Roon, M., Robanus-Maandag, E., te Riele, H., van der Valk, M., Deschamps, J., Sofroniew, M., van Lohuizen, M., et al. (1994). Posterior transformation, neurological abnormalities, and severe hematopoietic defects in mice with a targeted deletion of the bmi-1 proto-oncogene. Genes Dev. *8*, 757–769.

van Lohuizen, M., Verbeek, S., Scheijen, B., Wientjens, E., van der Gulden, H., and Berns, A. (1991). Identification of cooperating oncogenes in E μ-myc transgenic mice by provirus tagging. Cell *65*, 737–752.

Wada, R., Muraoka, N., Inagawa, K., Yamakawa, H., Miyamoto, K., Sadahiro, T., Umei, T., Kaneda, R., Suzuki, T., Kamiya, K., et al. (2013). Induction of human cardiomyocyte-like cells from fibroblasts by defined factors. Proc. Natl. Acad. Sci. USA *110*, 12667–12672.

Wamstad, J.A., Alexander, J.M., Truty, R.M., Shrikumar, A., Li, F., Eilertson, K.E., Ding, H., Wylie, J.N., Pico, A.R., Capra, J.A., et al. (2012). Dynamic and coordinated epigenetic regulation of developmental transitions in the cardiac lineage. Cell *151*, 206–220.

Wang, H., Wang, L., Erdjument-Bromage, H., Vidal, M., Tempst, P., Jones, R.S., and Zhang, Y. (2004). Role of histone H2A ubiquitination in Polycomb silencing. Nature *431*, 873–878.

Wang, L., Liu, Z., Yin, C., Asfour, H., Chen, O., Li, Y., Bursac, N., Liu, J., and Qian, L. (2015a). Stoichiometry of Gata4, Mef2c, and Tbx5 influences the efficiency and quality of induced cardiac myocyte reprogramming. Circ. Res. *116*, 237–244.

Wang, L., Liu, Z., Yin, C., Zhou, Y., Liu, J., and Qian, L. (2015b). Improved Generation of Induced Cardiomyocytes Using a Polycistronic Construct Expressing Optimal Ratio of Gata4, Mef2c and Tbx5. J. Vis. Exp. *105*, 53426.

Xin, M., Olson, E.N., and Bassel-Duby, R. (2013). Mending broken hearts: cardiac development as a basis for adult heart regeneration and repair. Nat. Rev. Mol. Cell Biol. *14*, 529–541.

Xue, Y., Ouyang, K., Huang, J., Zhou, Y., Ouyang, H., Li, H., Wang, G., Wu, Q., Wei, C., Bi, Y., et al. (2013). Direct conversion of fibroblasts to neurons by reprogramming PTB-regulated microRNA circuits. Cell *152*, 82–96.

Zhao, Y., Londono, P., Cao, Y., Sharpe, E.J., Proenza, C., O'Rourke, R., Jones, K.L., Jeong, M.Y., Walker, L.A., Buttrick, P.M., et al. (2015). High-efficiency reprogramming of fibroblasts into cardiomyocytes requires suppression of pro-fibrotic signalling. Nat. Commun. *6*, 8243.

Zhou, H., Dickson, M.E., Kim, M.S., Bassel-Duby, R., and Olson, E.N. (2015). Akt1/protein kinase B enhances transcriptional reprogramming of fibroblasts to functional cardiomyocytes. Proc. Natl. Acad. Sci. USA *112*, 11864–11869.